Surface buckling of black phosphorus: Determination, origin, and influence on electronic structure

Zhongwei Dai,[1,*] Wencan Jin,[2,†] Jie-Xiang Yu,[1] Maxwell Grady,[1] Jerzy T. Sadowski,[3] Young Duck Kim,[2,‡] James Hone,[2] Jerry I. Dadap,[2] Jiadong Zang,[1] Richard M. Osgood, Jr.,[2] and Karsten Pohl[1]

[1]*Department of Physics and Materials Science Program, University of New Hampshire, Durham, New Hampshire 03824, USA*

[2]*Columbia University, New York, New York 10027, USA*

[3]*Center for Functional Nanomaterials, Brookhaven National Laboratory, Upton, New York 11973, USA*

(Received 21 September 2017; published 29 December 2017)

The surface structure of black phosphorus materials is determined using surface-sensitive dynamical microspot low energy electron diffraction (μLEED) analysis using a high spatial resolution low energy electron microscopy (LEEM) system. Samples of (i) crystalline cleaved black phosphorus (BP) at 300 K and (ii) exfoliated few-layer phosphorene (FLP) of about 10 nm thickness which were annealed at 573 K in vacuum were studied. In both samples, a significant surface buckling of 0.22 Å and 0.30 Å, respectively, is measured, which is one order of magnitude larger than previously reported. As direct evidence for large buckling, we observe a set of (for the flat surface forbidden) diffraction spots. Using first-principles calculations, we find that the presence of surface vacancies is responsible for the surface buckling in both BP and FLP, and is related to the intrinsic hole doping of phosphoresce materials previously reported.

DOI: 10.1103/PhysRevMaterials.1.074003

I. INTRODUCTION

Black phosphorus (BP), together with its monolayer version known as phosphorene, has had a recent rebirth as a new member of the vigorously studied two-dimensional (2D) materials family. It has attracted much attention due to its intriguing potential applications for modern electronics [1–4] and photonics [5,6]. For example, BP exhibits an intrinsic layer-dependent band gap ranging from 0.3 eV (bulk) to 2 eV (monolayer) [7], and thus bridges the energy gap between graphene and transition metal dichalcogenides (TMDs) [8]. This strong layer dependence presents the potential for integrated devices on a single supporting platform. Despite the surge of research in the applications of BP, much remains to be learned of its basic physical properties both from a device and a fundamental physics perspective. For example, the origin of the previously measured intrinsic p-type nature of BP is unknown [1,3]; existing first-principles calculations could not completely explain measured band structures of BP [9,10]. The electronic properties are inherently related to the atomic crystal structures, and when thinned down to a few-layer form, the surface structures play an important role in the electronic properties of 2D materials.

However, to date, there is no consensus on the atomic structure of the surface region of BP. The crystal structure of BP, as shown in Fig. 1, has a puckered honeycomb structure similar to that of graphene [11]. Two previous STM studies of phosphorene [12,13] have revealed important aspects of the BP surface topography and observed an apparent height difference between two symmetrically equivalent atoms P_1 and P_2, as shown in Fig. 1(d). While these STM measurements were not able to quantify the geometrical height difference between P_1 and P_2, denoted as surface buckling, these studies proposed very small surface buckling values, 0.02 Å [12] and 0.06 Å [13], based on their first-principles calculations. In order to experimentally resolve the surface atomic structure of BP, two main challenges for the characterization technique have to be overcome: it has to be (i) nondestructive and sensitive to the 3D atomic structure in the first few layers, and (ii) able to restrict the lateral sampling area to a few μm because many 2D materials including phosphorene are commonly prepared as small flakes. Here, selected area microspot low energy electron diffraction (μLEED) in a low energy electron microscope (LEEM), combined with dynamical intensity versus incoming electron energy (LEED-*IV*) calculations, is one of the very few practical techniques able to determine the 3D surface structure and composition of 2D materials with atomic resolution [14–18].

In this report, we present a detailed experimental atomic surface structure determination of BP. We produce pristine BP surfaces by controlled evaporation of the surface oxide layers. LEEM and dynamical μLEED-*IV* analysis are employed to examine the *in situ* cleaved bulk BP surface and mechanically exfoliated few-layer phosphorene (FLP) flakes of about 10 nm thickness. These measurements indicate that the surface bucklings for the two studied systems are 0.22 Å and 0.30 Å, respectively, which are one order of magnitude larger than two previously reported theoretical values. Finally we use first-principles calculations to identify that the presence of surface vacancies is very likely the origin of not only the surface buckling in BP but also the intrinsic hole doping of phosphorene that was reported previously [3,19].

II. LEEM/μLEED EXPERIMENTS AND DYNAMICAL LEED-*IV* ANALYSIS

Our experiments were carried out in the Elmitec AC-LEEM and LEEM V systems at the Center for Functional Nanomaterials in Brookhaven National Laboratory. The spatial resolution in LEEM mode is better than 3 nm and the electron beam spot size is 2 μm in diameter in the μLEED mode. Single-crystal bulk BP was cleaved in ultrahigh vacuum at

*zbr5@wildcats.unh.edu

†Current address: Department of Physics, University of Michigan, Ann Arbor, Michigan 48109, USA.

‡Current address: Department of Physics, Kyung Hee University, Seoul 02447, Republic of Korea.

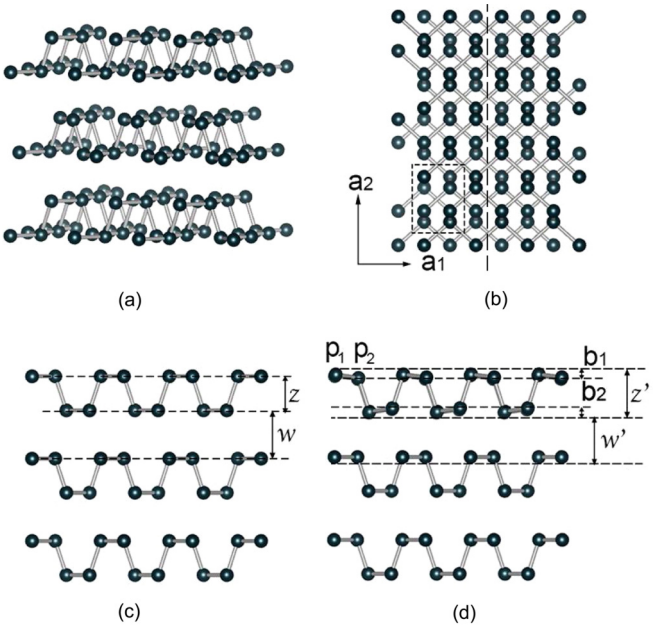

FIG. 1. (a)–(c) BP bulk crystal structure: 3D rendering, top view, and side view along the dashed line in (b), respectively. (d) Side view of BP and FLP relaxed surface structure, along dashed line in (b). Dotted square in (b) indicates the unit cell of BP, containing 8 P atoms.

room temperature. Figure 2(a) shows the real-space bright field LEEM image of a freshly cleaved BP surface. μLEED data were acquired at the region denoted by the red 2 μm circle using a normal incident electron beam. Figure 2(b) shows the well-defined LEED pattern at 35 eV electron energy, indicating a very well ordered surface. To prepare our FLP samples, black phosphorous flakes were mechanically exfoliated onto n-doped Si chips with native oxide, using a previously described method [20,21]. The substrate was pre-patterned with gold marks, which allowed for locating and characterizing the flakes of interest using an optical microscope; see Fig. 2(c). This procedure was performed in a Ne atmosphere. Subsequently, the sample was encapsulated and transferred to the LEEM chamber. The total exposure time of the exfoliated sample to air was less than 5 minutes. Even with such a short exposure time, significant surface oxidization and contamination was observed using photoemission electron microscopy (PEEM). In order to remove the surface oxide layers, we annealed the sample at 300 °C in ultrahigh vacuum for 2 hours. As shown in PEEM and LEEM images, Figs. 2(d)–2(e), the surface was pristine and uniform after successful annealing. Figure 2(f) shows the sharp LEED pattern at 35 eV electron energy, indicating a very well ordered layered structure. To fully investigate the surface atomic structure we collected μLEED-*IV* spectra for 7 recorded diffraction spots with an electron energy range of 25 to 135 eV for both sample varieties. The intensities of symmetrically equivalent beams were averaged to minimize intensity anisotropy of the diffraction beam due to possible small sample titling (<0.1°). Specifically, as shown in Figs. 2(b) and 2(f), intensities of spots A were averaged to assign the (01) diffraction beam and beam intensities of spots B were averaged to assign the (11) diffraction beam. The

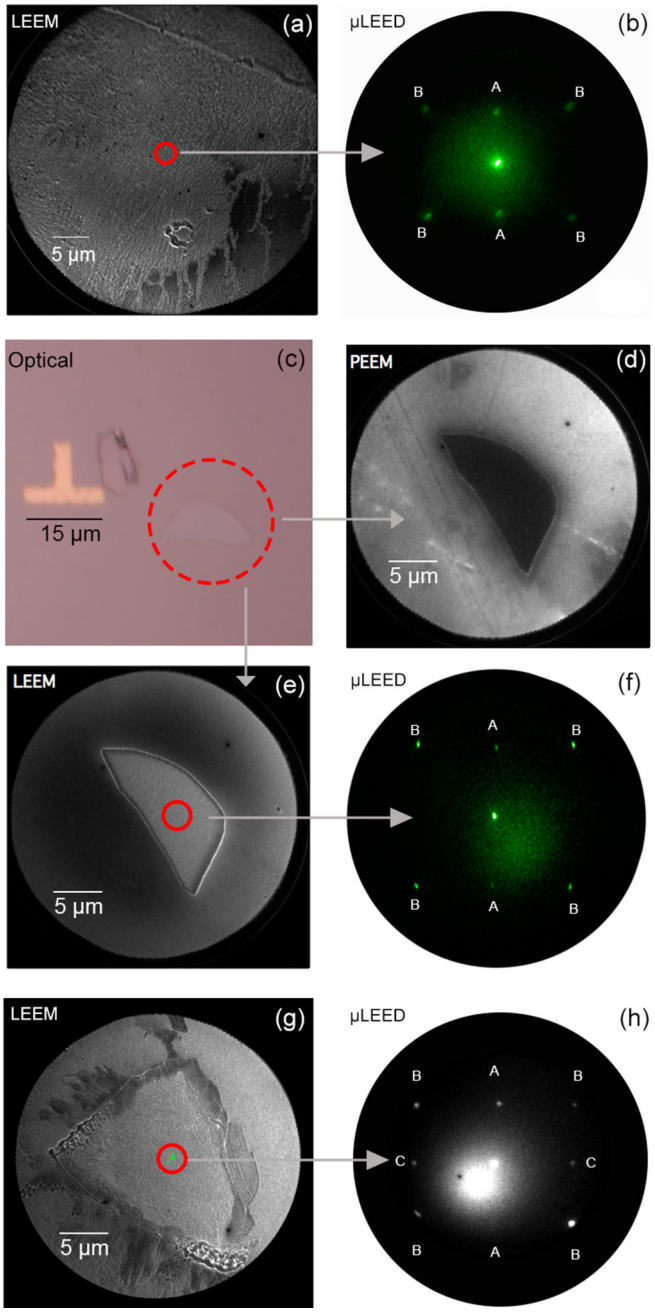

FIG. 2. (a) LEEM image and (b) μLEED diffraction pattern of red-circled area in (a) taken at 30 eV electron energy of freshly cleaved BP crystal surface. (c) Optical, (d) PEEM, (e) LEEM, and (f) μLEED image of red-circled area in (e) taken at 30 eV electron energy of mechanically exfoliated flake of FLP, of about 10 nm thickness. (g) LEEM image and (h) μLEED diffraction pattern of an exfoliated flake after annealing at 370 °C, taken at 24 eV electron energy. Sharp diffraction pattern indicates that the surface is pristine and well ordered. An extra set of "forbidden spots," the (10) beams denoted as C in (g), is clearly visible and unequivocal evidence of surface buckling on BP.

background intensity was then subtracted from the diffraction beam intensity.

Dynamical LEED-*IV* analysis was carried out to extract the surface atomic structural information for bulk BP and FLP

from the corresponding μLEED-*IV* curves. In a dynamical LEED-*IV* analysis, *IV* curves are calculated for a trial structure and compared with experimental curves. A χ^2-based R_2 reliability factor is used to quantify the difference between calculated and experimental *IV* curves [22]. The surface structural parameters are then adjusted in the search for the optimized surface structure that minimizes the R_2 factor. For electrons with an energy range of 25–135 eV, the mean-free path is about 5 to 10 Å. Use of this energy range means that our μLEED-*IV* curves are most sensitive to the structural parameters of the top two phosphorene layers, i.e., the buckling of the top atomic layer b_1, the thickness of the first phosphorene layer z', the buckling of the bottom atomic layer b_2, and the van der Waals gap between the top and second phosphorene layer w', as demonstrated in Fig. 1(d).

Multiple-scattering theory and a muffin-tin potential model were implemented to calculate the LEED-*IV* curves [23,24]. We used computer codes from Adams *et al.* [22], which were developed from the programs of Pendry [23] and Van Hove and Tong [24]. The utilization of the R_2 factor allows for the relative intensities of the diffraction beams to be preserved during the optimization, which enhances the reliability of the surface structure determination. The phase shifts (a quantity describing the atomic scattering property [24]) were calculated using the Barbieri/Van Hove phase shift calculation package [25]. The muffin-tin radii for phosphorus atoms was set to $r_P^{MT} = 2.099$ a.u. and 12 phase shifts ($L = 11$) were used for the LEED-*IV* calculation. The in-plane lattice constants were set to $a_1 = 3.313$ Å and $a_2 = 4.374$ Å, the thickness of the phosphorene layer to $z = 2.166$ Å, and the van der Waals distance between phosphorene layers to $w = 3.071$ Å for the bulk, as indicated in Fig. 1 [11].

The mean-squared atomic vibrational displacements $\langle u^2\rangle_T$ for the P atoms were calculated individually according to the relation between Debye temperature θ_D and $\langle u^2\rangle_T$ at the sample temperature of $T = 300$ K for bulk BP and $T = 573$ K for the FLP flakes using the following equation [23]:

$$\langle u^2\rangle_T = \frac{9\hbar^2}{m_a k_B \theta_D}\left(\frac{T^2}{\theta_D^2}\int_0^{\frac{\theta_D}{T}}\frac{x\,dx}{e^x-1}+\frac{1}{4}\right), \qquad (1)$$

where m_a is the atomic mass, $\hbar$ is the Planck's constant, and k_B is the Boltzmann constant. The Debye temperature θ_D was set to 550 K [26]. The inner potential, $V_0 + iV_{im}$, was set to be independent of energy. The real part V_0 was initially set to 8 eV and adjusted through ΔV_0 during the fitting process while the imaginary part V_{im} was fixed at 6 eV.

Best-fit structural parameter values are listed in Table I and compared with previously reported results [12,13]. The calculated LEED-*IV* curves using optimized structural parameters match well with the experimental curves for both the BP crystal surface at 300 K and exfoliated FLP flake at 573 K, as shown in Figs. 3(a)–3(d). The minimized R_2 factors are 0.03 and 0.02, respectively. For comparison, the calculated *IV* curves [blue dashed lines in Figs. 3(a) and 3(b)] using a flat, unbuckled surface are distinctively different from our experimental results. For the freshly cleaved BP crystal surface, our results show that the top-layer surface buckling b_1 is 0.22 Å and the second phosphorus atomic layer buckling b_2 is 0.27 Å. The thickness of the top phosphorene layer z' is expanded by 5.3% from its bulk value of 2.166 Å. The van der Waals gap between the top and second phosphorene layer w' is contracted by 8% from its bulk value of 3.071 Å. For the mechanically exfoliated flake of FLP at 573 K, the top and second layer buckling are 0.30 Å and 0.29 Å, respectively. The surface bucklings are slightly larger at 573 K than the BP crystal surface at 300 K. We attribute this increase of surface buckling to thermal surface expansion at elevated temperature. For the same reason, the top phosphorene layer z' and the top van der Waals gap w' are also slightly increased at 573 K compared to 300 K. z' shows an expansion of 9.9% and w' a contraction of 6.3%, with respect to their corresponding bulk values. Due to the small data set and the very low *R* factors it is difficult to assign meaningful uncertainties to the optimized individual structural parameters. Figure 3(e) and 3(f) show plots of the reliability R_2 factor as a function of the surface buckling b_1 and the second atomic layer buckling b_2 for both of the investigated samples. Well-defined minima were observed for both cases. Along with the good agreement of experimental and calculated *IV* curves, both results give us confidence in our findings.

The most striking result is that the BP surface buckling b_1 is one order of magnitude larger than the previously proposed theoretical values [12,13], for both BP and FLP samples investigated. Note that the buckling extends to the second atomic layer. Similar significant surface buckling has also been predicted for other group V thin film materials such as Bi and other similar elemental 2D materials such as silicene and germanene by various first-principles studies. Specifically, Cahangirov *et al.* predicted that the buckling height for silicene is 0.44 Å and 0.64 Å [27]; Sadowski *et al.* proposed the buckling of Bi thin film is 0.5 Å [28,29].

Another exfoliated BP flake of about 100 nm thickness was studied for *in situ* observation of the surface annealing at different temperatures using LEEM. The surface crystallinity was monitored using μLEED with beam spot size of 2 μm. As described in detail in the Supplemental Material [30], the surface of freshly exfoliated flakes, as shown in Fig. S1, were immediately covered with an oxidized layer even with less than 10 min exposure to air. The oxide layer started to evaporate at around 250 °C, as shown in Fig. S1, panels (e)–(i). The surface layer was completely removed by further annealing up to 370 °C, and a pristine surface was produced, as confirmed by the sharp LEED pattern, shown in Figs. 2(g) and 2(h). Moreover, a set of (for the unbuckled surface forbidden) diffraction spots, the (10) beams denoted by C in Fig. 2(h), was present. This is direct evidence of the surface glide symmetry breaking due to the height difference of P_1 and P_2, i.e., surface buckling. We want to note that the (10) spots are significantly

TABLE I. Optimum parameter values for the surface structure of BP crystal and exfoliated BP flake.

Model	T	b_1 (Å)	b_2 (Å)	z' (Å) ($\Delta z/z$)	w' (Å) ($\Delta w/w$)
Cleaved BP	300 K	0.225	0.269	2.287 (+5.3%)	2.825 (−8.0%)
FLP	573 K	0.300	0.290	2.381 (+9.9%)	2.877 (−6.3%)
DFT [12]		0.02			
DFT [13]		0.06			

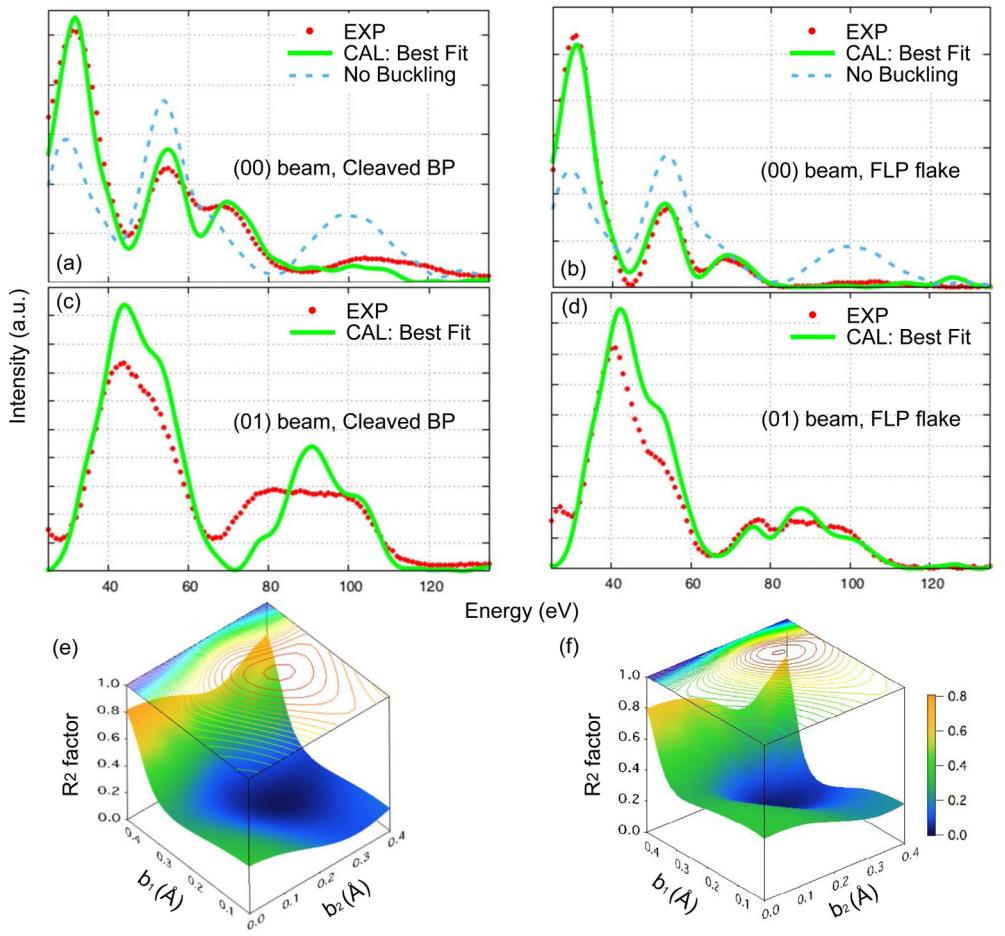

FIG. 3. (a)–(d) (00) and (01) low-electron energy diffraction beam *IV* curves for cleaved BP crystal and exfoliated FLP flake, respectively. Red dotted curves are experimental and green solid curves are calculated using optimized surface structural parameters. (e), (f) Reliability R_2 factor plotted vs b_1 and b_2 for cleaved BP crystal and exfoliated FLP flake, respectively.

weaker in intensity than the other diffraction spots and can be easily missed. In fact, they are only observable in the small energy window of 23–25 eV; see Fig. S2(b).

III. DFT CALCULATIONS

In order to support the measured significant buckling and reveal its origin, first-principles calculations were employed. Calculations were carried out based on the framework of density functional theory (DFT) with the projector augmented wave (PAW) potential [31] as implemented in the Vienna *ab initio* simulation package (VASP) [32–34]. The plane-wave functions expanded with an energy cutoff of 400 eV were employed throughout calculations. The exchange-correlation energy was described by the generalized gradient approximation (GGA) in the Perdew, Burke, and Ernzerhof (PBE) form [35]. The k points in the two-dimensional Brillouin zone (BZ) of the 1×1 unit cell of monolayer BP containing 4 phosphorous atoms were sampled on a 16×12 mesh. The van der Waals (vdW) interactions were also incorporated within the Tkatchenko-Scheffler method [36]. In addition, we employed the Heyd, Scuseria, and Ernzerhof (HSE06) hybrid functional [37,38] for the band structure calculations.

The structure of monolayer phosphorene and the top phosphorene layer of bulk BP (a six-layer supercell) were calculated and compared. Only very small structural differences were observed, <0.001 Å, between the atomic positions and bond lengths of the monolayer phosphene and that of the top layer of bulk. This is expected for layered materials with weak van der Waals bonding in between adjacent layers. In order to simplify our calculations, we focus on single-layer phosphorene. However, final model structures were compared against consistency calculations for two-bilayer phosphorene and no signs of interactions other than van der Waals were found. The thickness of the vacuum layer in each slab structure is more than 15 Å.

First, defect-free monolayer phosphorene with different supercell sizes was investigated. The lattice structure was optimized until the atomic force, both Hellmann-Feynman and vdW terms included, on each relaxed atom was less than 1 meV/Å. In an up to 8×4 supercell, no buckling was found within the accuracy of the calculation. This result is reasonable since both BP bulk and monolayer structures have the insulating electronic structures with band gaps, and exposed surfaces do not bring about the electronic mismatch or additional dangling bonds. Surface reconstruction is thus not necessary in such a stable structure.

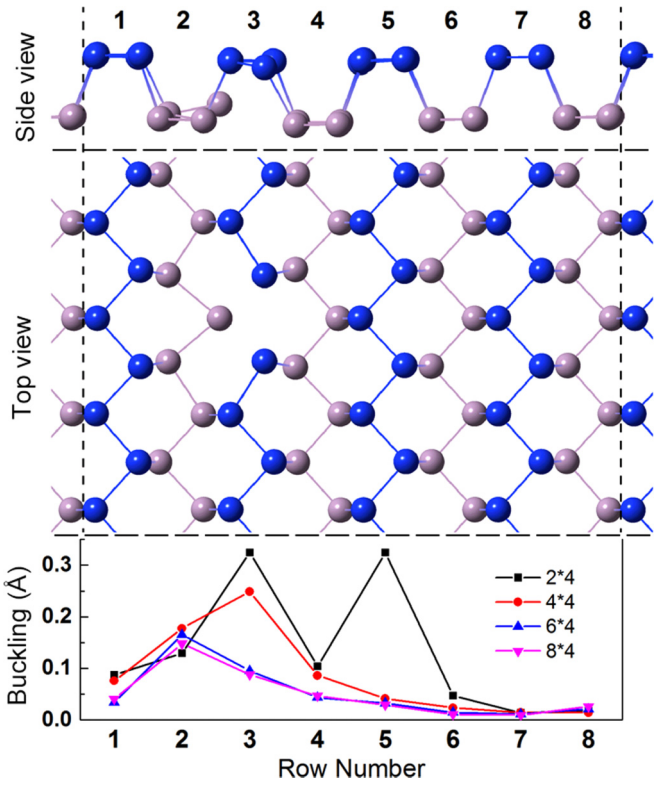

FIG. 4. Phosphorene atomic structure with defect introduced. Upper panels: Side and top view of an $n \times 4$ ($n = 2, 4, 6, 8$) supercell of the monolayer phosphorene with a point defect introduced at row 3. Blue and gray colors of balls distinguish the top and second P atomic layers. Lower panel: Average magnitude of buckling in each row for various $n \times 4$ supercells.

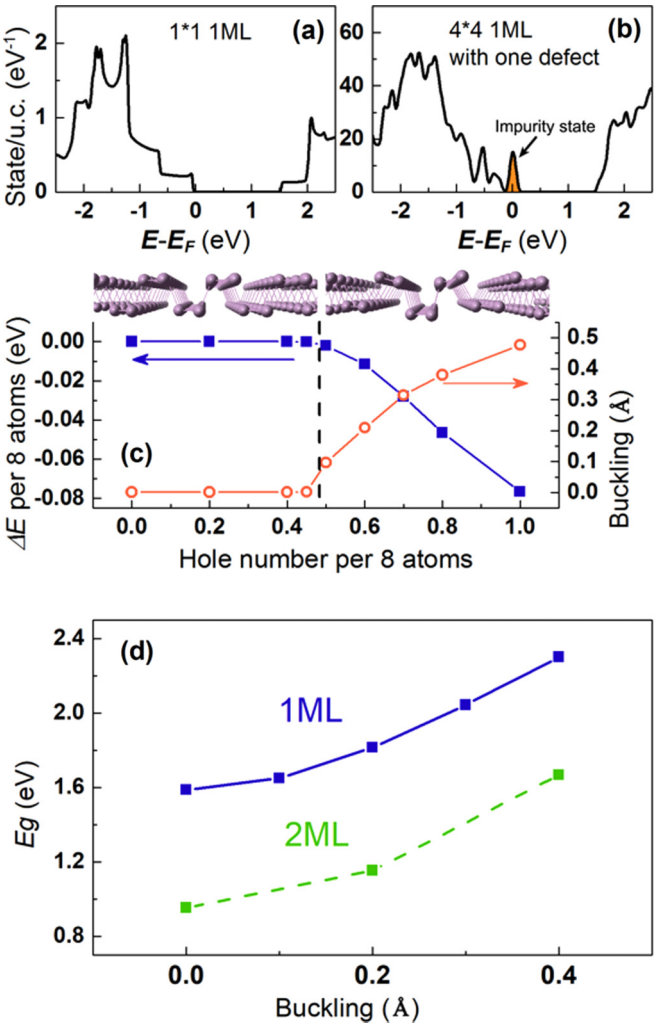

FIG. 5. Buckling and hole doping induced by defects. The DOS for (a) the ideal monolayer and (b) the 4×4 defect-included supercell BP. The Fermi level is set to zero. (c) Energy difference (blue solid squares) between the buckled and nonbuckled configurations and the magnitude of buckling (red open circles) with increasing hole-doping number. (d) Dependence of band gap on the buckling magnitude in monolayer (blue solid line) and bilayer (green dashed line) phosphorenes. The magnitude of the buckling is adjusted in single-layer phosphorene (1 ML) and the top bilayer of two-layer phosphorene (2 ML) from the range of 0 Å to 0.4 Å. The band gap of each structure is calculated accordingly and shown in (d).

However, if an impurity, such as a vacancy defect [13] or doping [3,19], is induced on the surface, the situation changes completely. In fact, Liang *et al.* have recently observed vacancy defects on their freshly cleaved surfaces of BP crystals [13] using STM. Here, we introduced a single point defect into the monolayer phosphorene by removing one atom. Several supercells were calculated with their sizes ranging from 2×4 to 8×4. After the structure optimization, deviations of the atoms along the out-of-plane direction were observed in all of these structures. As shown in the top view (middle panel) of Fig. 4, each supercell has 8 zigzag rows, and the defect is located on the upper layer of row 3. The magnitude of buckling in each row is summarized in the bottom panel of Fig. 4 by calculating the standard deviations of the phosphorus atoms' z components for each entire row. It is seen that the buckling is maximized in rows around the defect, and the maximum buckling ranges from 0.15 Å to 0.33 Å through all the supercell sizes under investigation. These calculations agree well with our experimental values of 0.22 Å to 0.30 Å. Although the buckling magnitude decays rapidly along the armchair direction, away from the row, on which the defect is located, no significant decay in the buckling magnitude was found in the zigzag direction. Based on these results, it is concluded that the buckling is significantly enhanced near the point defect. It is anisotropic and long-range along the zigzag direction while it is short-range along the armchair direction. The defect-induced buckling cannot be maintained in the armchair direction. This interesting insight agrees well with the recent experimental observation of an anisotropy in the surface density of states (DOS) on the BP surface by STM [13].

Intuitively, one would expect that such long-range buckling would be reflected in the band structures as well. Thus the electronic structure of the 4×4 supercell with a single vacancy was investigated and compared with that of a clean monolayer. According to the density of state results shown in Figs. 5(a) and 5(b), the clean monolayer BP is insulating with a band gap of 1.5 eV, while an impurity state is present in the defect-containing supercell across the Fermi level close to the top

of valence states. A similar state was also observed by Zhang *et al.* [12] in their STM dI/dV measurement. This indicates the existence of the defect-induced hole-doping electronic structure in these defect structures; i.e., each phosphorus vacancy generates three dangling bonds that need to be saturated by more electrons. This suggests that the distortion of the lattice, such as buckling, appears in order to eliminate this instability of the electronic structure.

To better understand the relation between hole doping and the surface structure of BP, the hole-doped 2×1 clean supercell structures with a tunable total electron number were optimized. As shown in Fig. 5(c), buckling appears when the hole number exceeds 0.5 per 8 phosphor atoms. The magnitude of the buckling as well as the energy difference between the buckled and ideal structures increases rapidly with the rise of the hole number. In particular, the buckling reaches 0.2 Å when the hole number is 0.6 per 8 atoms. Our first-principles calculations thus show that the presence of defects induces hole doping on the clean BP surface, which in turn leads to lattice distortion and the surface buckling. It was confirmed experimentally that both undoped bulk BP [19] and FLP [3] are p-type semiconductors, but the origin of intrinsic p-type doping is unclear so far. Recently, Osada proposed that the edge state of finite bilayer phosphorene might be the origin of the intrinsic hole doping around the edge [39]. Our DFT calculations, together with the experimental observation of BP surface reconstruction, strongly indicate that the presence of surface defects is a likely explanation for the intrinsic hole doping for both bulk BP and FLP.

IV. CONCLUSIONS

To summarize, we observed that significant oxidization of exfoliated BP flakes occurs even after short exposure to air, but the oxide layer can be efficiently removed by annealing at 250 °C to 370 °C. Using high spatial resolution LEEM and unique μLEED-*IV* analysis, the significant surface buckling on the top pristine BP surface and the associated symmetry breaking are directly observed in the form of additional diffraction spots in the LEED pattern, and the surface buckling is quantitatively measured. It is 0.22 Å for the cleaved bulk flake and 0.30 Å in the 10 nm thick FLP flake. A similar buckling for the second phosphorus layer was identified, which is accessible by highly subsurface-sensitive μLEED-*IV*. Using first-principles calculations, we further confirmed our surface structural results and proposed a vacancy defect driven mechanism for the surface buckling. The surface vacancy defect also introduces an impurity state in the band gap, and is consistent with previous reports of the intrinsic p-type nature of phosphorene materials. Recently, vacancy defects in similarly cleaved BP surfaces were reported in STM/STS measurements [40,41].

The surface buckling addressed in this work can be used to modify the band gap of thin BP flakes and may lead to future electronic applications. As shown in Fig. 5(d), buckling indeed increases the band gap at the Γ point for both monolayer and bilayer phosphorenes. The band gaps increase from 1.59 eV to 2.30 eV for monolayer and from 0.95 eV to 1.67 eV for two-bilayer phosphorene when a buckling of 0.4 Å is introduced in the top layer. Even with a limited data set of buckling magnitudes at different temperatures, our measurement indicates a possible temperature dependence of the observed surface buckling. Previous studies have shown anomalous temperature dependence of the band gap in both phosphorene [42] and bulk black phosphorus [43,44], which may lead to BP-based thermoelectric devices, and more detailed studies are needed.

ACKNOWLEDGMENTS

The experimental work presented here was carried out at the Center for Functional Nanomaterials, which is a U.S. Department of Energy (DOE) Office of Science Facility, at Brookhaven National Laboratory under Contract No. DE-SC0012704. The work of Z.D. and K.P. was supported by NSF DMR-1006863. First-principles calculations by J.X.Y. and J.Z. were supported by the U.S. Department of Energy (DOE), Office of Science, Basic Energy Sciences (BES) under Award No. DE-SC0016424 and used the Extreme Science and Engineering Discovery Environment (XSEDE) under Grant No. TG-PHY170023. In addition, the work of R.M.O., W.J., and J.I.D. was financially supported by the US Department of Energy under Contract No. DE-FG 02-04-ER-46157. The work of J.H. and Y.D.K. was financially supported by the NSF MRSEC program through Columbia University at the Center for Precision Assembly of Superstratic and Superatomic Solids (NSF DMR-1420634).

[1] L. Li, Y. Yu, G. J. Ye, Q. Ge, X. Ou, H. Wu, D. Feng, X. H. Chen, and Y. Zhang, Nat. Nanotechnol. **9**, 372 (2014).
[2] F. Xia, H. Wang, and Y. Jia, Nat. Commun. **5**, 4458 (2014).
[3] H. Liu, A. T. Neal, Z. Zhu, Z. Luo, X. Xu, D. Tománek, and P. D. Ye, ACS Nano **8**, 4033 (2014).
[4] H. Wang, X. Wang, F. Xia, L. Wang, H. Jiang, Q. Xia, M. L. Chin, M. Dubey, and S. Han, Nano Lett. **14**, 6424 (2014).
[5] Y. Deng, Z. Luo, N. J. Conrad, H. Liu, Y. Gong, S. Najmaei, P. M. Ajayan, J. Lou, X. Xu, and P. D. Ye, ACS Nano **8**, 8292 (2014).
[6] M. Buscema, D. J. Groenendijk, G. A. Steele, Herre S. J. van der Zant, and A. Castellanos-Gomez, Nat. Commun. **5**, 4651 (2014).
[7] V. Tran, R. Soklaski, Y. Liang, and L. Yang, Phys. Rev. B **89**, 235319 (2014).
[8] X. Ling, H. Wang, S. Huang, F. Xia, and M. S. Dresselhaus, Proc. Natl. Acad. Sci. USA **12**, 4523 (2015).
[9] C. Q. Han, M. Y. Yao, X. X. Bai, L. Miao, F. Zhu, D. D. Guan, S. Wang, C. L. Gao, C. Liu, D. Qian, Y. Liu, and J.-F. Jia, Phys. Rev. B **90**, 085101 (2014).
[10] A. Carvalho, M. Wang, X. Zhu, A. S. Rodin, H. Su, and A. H. C. Neto, Nat. Rev. Mater. **1**, 16061 (2016).
[11] A. Morita, Appl. Phys. A **39**, 227 (1986).
[12] C. D. Zhang, J. C. Lian, W. Yi, Y. H. Jiang, L. W. Liu, H. Hu, W. D. Xiao, S. X. Du, L. L. Sun, and H. J. Gao, J. Phys. Chem. C **113**, 18823 (2014).

[13] L. Liang, J. Wang, W. Lin, B. G. Sumpter, V. Meunier, and M. Pan, Nano Lett. **14**, 6400 (2014).
[14] Z. Dai, W. Jin, M. Grady, J. T. Sadowski, J. I. Dadap, R. M. Osgood, Jr., and K. Pohl, Surf. Sci. **600**, 16 (2017).
[15] W. Jin, S. Vishwanath, J. Liu, L. Kong, R. Lou, Z. Dai, J. T. Sadowski, X. Liu, H.-H. Lien, J. Ma, T. Qian, J. I. Dadap, K. Pohl, S. Wang, J. Furdyna, H. Ding, H. G. Xing, and R. M. Osgood, Jr., Phys. Rev. X **7**, 041020 (2017).
[16] J. de la Figuera, J. Puerta, J. Cerda, F. E. Gabaly, and K. McCarty, Surf. Sci. **600**, L105 (2006).
[17] J. Sun, J. B. Hannon, G. L. Kellogg, and K. Pohl, Phys. Rev. B **76**, 205414 (2007).
[18] J. B. Hannon, J. Sun, K. Pohl, and G. L. Kellogg, Phys. Rev. Lett. **96**, 246103 (2006).
[19] Y. Akahama, S. Endo, and S. Narita, J. Phys. Soc. Jpn. **52**, 2148 (1983).
[20] W. Jin, P.-C. Yeh, N. Zaki, D. Zhang, J. T. Sadowski, A. Al-Mahboob, A. M. van der Zande, D. A. Chenet, J. I. Dadap, I. P. Herman, P. Sutter, J. Hone, and R. M. Osgood, Jr., Phys. Rev. Lett. **111**, 106801 (2013).
[21] W. Jin, P.-C. Yeh, N. Zaki, D. Zhang, J. T. Liou, J. T. Sadowski, A. Barinov, M. Yablonskikh, J. I. Dadap, P. Sutter, I. P. Herman, and R. M. Osgood, Jr., Phys. Rev. B **91**, 121409 (2015).
[22] D. L. Adams, Surf. Sci. **519**, 157 (2002).
[23] J. B. Pendry, *Low-Energy Electron Diffraction* (Academic, London, 1974).
[24] M. Van Hove and S. Y. Tong, *Surface Crystallography by LEED* (Springer-Verlag, Berlin, 1979).
[25] A. Barbieri and M. Van Hove, packages available online at http://www.icts.hkbu.edu.hk/vanhove/.
[26] C. Kaneta, H. Katayama-Yoshida, and A. Morita, Solid State Commun. **44**, 613 (1982).
[27] S. Cahangirov, M. Topsakal, E. Aktürk, H. Şahin, and S. Ciraci, Phys. Rev. Lett. **102**, 236804 (2009).
[28] J. T. Sadowski, T. Nagao, S. Yaginuma, Y. Fujikawa, and T. Sakurai, J. Appl. Phys. **99**, 014904 (2006).
[29] T. Nagao, J. T. Sadowski, M. Saito, S. Yaginuma, Y. Fujikawa, T. Kogure, T. Ohno, Y. Hasegawa, S. Hasegawa, and T. Sakurai, Phys. Rev. Lett. **93**, 105501 (2004).
[30] See Supplemental Material at http://link.aps.org/supplemental/10.1103/PhysRevMaterials.1.074003 for *in situ* LEEM observation of the evaporation of the surface oxide layer on exfoliated black phosphorus flake, LEED analysis of the origin of the "forbidden" (10) diffraction spots, and DFT calculation of monolayer phosphorene band structure with and without buckling.
[31] P. E. Blöchl, Phys. Rev. B **50**, 17953 (1994).
[32] G. Kresse and J. Furthmüller, Comput. Mater. Sci. **6**, 15 (1996).
[33] G. Kresse and J. Furthmüller, Phys. Rev. B **54**, 11169 (1996).
[34] G. Kresse and D. Joubert, Phys. Rev. B **59**, 1758 (1999).
[35] J. P. Perdew, K. Burke, and M. Ernzerhof, Phys. Rev. Lett. **77**, 3865 (1996).
[36] A. Tkatchenko and M. Scheffler, Phys. Rev. Lett. **102**, 073005 (2009).
[37] J. Heyd, G. E. Scuseria, and M. Ernzerhof, J. Chem. Phys. **118**, 8207 (2003).
[38] J. Heyd, G. E. Scuseria, and M. Ernzerhof, J. Chem. Phys. **124**, 219906 (2006).
[39] T. Osada, J. Phys. Soc. Jpn. **84**, 013703 (2015).
[40] B. Kiraly, N. Hauptmann, A. N. Rudenko, M. I. Katsnelson, and A. A. Khajetoorians, Nano Lett. **17**, 3607 (2017).
[41] J. V. Riffle, C. Flynn, B. St. Laurent, C. A. Ayotte, C. A. Caputo, and S. M. Hollen, arXiv:1712.08491 [cond-mat.mes-hall].
[42] A. Surrente, A. A. Mitioglu, K. Galkowski, W. Tabis, D. K. Maude, and P. Plochocka, Phys. Rev. B **93**, 121405 (2016).
[43] D. Warschauer, J. Appl. Phys. **34**, 1853 (1963).
[44] M. Baba, Y. Nakamura, K. Shibata, and A. Morita, Jpn. J. Appl. Phys. **30**, L1178 (1991).